



# Endoplasmic Reticulum Luminal Indicators in *Drosophila* Reveal Effects of HSP-Related Mutations on Endoplasmic Reticulum Calcium Dynamics

Megan K. Oliva<sup>1\*</sup>, Juan José Pérez-Moreno<sup>1</sup>, Jillian O'Shaughnessy<sup>1</sup>, Trevor J. Wardill<sup>2</sup> and Cahir J. O'Kane<sup>1\*</sup>

<sup>1</sup> Department of Genetics, University of Cambridge, Cambridge, United Kingdom, <sup>2</sup> College of Biological Sciences, University of Minnesota, Minneapolis, MN, United States

## OPEN ACCESS

### Edited by:

Xin Qi,  
Case Western Reserve University,  
United States

### Reviewed by:

Antonio Orlacchio,  
Santa Lucia Foundation (IRCCS), Italy  
Brandon K. Harvey,  
National Institute on Drug Abuse  
(NIDA), United States

### \*Correspondence:

Megan K. Oliva  
megan.k.oliva@gmail.com  
Cahir J. O'Kane  
c.okane@gen.cam.ac.uk

### Specialty section:

This article was submitted to  
Neurodegeneration,  
a section of the journal  
Frontiers in Neuroscience

**Received:** 18 February 2020

**Accepted:** 10 July 2020

**Published:** 10 August 2020

### Citation:

Oliva MK, Pérez-Moreno JJ,  
O'Shaughnessy J, Wardill TJ and  
O'Kane CJ (2020) Endoplasmic  
Reticulum Luminal Indicators  
in *Drosophila* Reveal Effects  
of HSP-Related Mutations on  
Endoplasmic Reticulum Calcium  
Dynamics. *Front. Neurosci.* 14:816.  
doi: 10.3389/fnins.2020.00816

Genes for endoplasmic reticulum (ER)-shaping proteins are among the most commonly mutated in hereditary spastic paraplegia (HSP). Mutation of these genes in model organisms can lead to disruption of the ER network. To investigate how the physiological roles of the ER might be affected by such disruption, we developed tools to interrogate its Ca<sup>2+</sup> signaling function. We generated GAL4-driven Ca<sup>2+</sup> sensors targeted to the ER lumen, to record ER Ca<sup>2+</sup> fluxes in identified *Drosophila* neurons. Using *GAL4* lines specific for Type Ib or Type Is larval motor neurons, we compared the responses of different luminal indicators to electrical stimulation, in axons and presynaptic terminals. The most effective sensor, ER-GCaMP6-210, had a Ca<sup>2+</sup> affinity close to the expected ER luminal concentration. Repetitive nerve stimulation generally showed a transient increase of luminal Ca<sup>2+</sup> in both the axon and presynaptic terminals. Mutants lacking neuronal reticulon and REEP proteins, homologs of human HSP proteins, showed a larger ER luminal evoked response compared to wild type; we propose mechanisms by which this phenotype could lead to neuronal dysfunction or degeneration. Our lines are useful additions to a *Drosophila* Ca<sup>2+</sup> imaging toolkit, to explore the physiological roles of ER, and its pathophysiological roles in HSP and in axon degeneration more broadly.

**Keywords:** hereditary spastic paraplegia, endoplasmic reticulum, calcium imaging, *Drosophila*, neurodegeneration

## INTRODUCTION

Hereditary spastic paraplegia (HSP) is a genetically heterogeneous disorder, with over 80 loci and 60 genes identified. It also shows phenotypic heterogeneity in manifestations such as age of onset and the presence of other symptoms (Blackstone, 2018). Despite this heterogeneity, there is evidence for some common mechanisms of cellular pathophysiology. The endoplasmic reticulum (ER) is implicated in these mechanisms, with HSP mutations affecting ER proteins

with a variety of roles including lipid metabolism, ER membrane-contact-site function, and ER architecture (Blackstone, 2018). Gene products that shape the tubular ER network are among the most commonly mutated in HSP, and mutation of these genes in model organisms leads to physical disruption of the ER network (O'Sullivan et al., 2012; Fowler and O'Sullivan, 2016; Summerville et al., 2016; Yalçın et al., 2017; Lindhout et al., 2019). These studies point to the importance of a continuous and connected tubular ER network throughout axons and presynaptic terminals and suggest disruption to this network as a common thread in HSP pathogenesis. Although changes in synaptic structure and function are found in these mutants (Summerville et al., 2016; Li et al., 2017; Lindhout et al., 2019), the direct physiological consequences of altered ER architecture remain elusive. It is imperative to understand the roles of ER architecture and the consequences of disrupting it, to understand how this might result in a neurodegenerative cascade.

We therefore need tools to study the physiological functions of axonal and presynaptic ER that depend on its architecture. Recently, de Juan-Sanz et al. (2017) developed sensitive genetically encoded calcium indicators (GECIs) targeted to the ER lumen, to examine the role of the ER in  $Ca^{2+}$  handling and signaling in synaptic activity in mammalian cultured neurons. In parallel to our work, Handler et al. (2019) used one of these sensors (ER-GCaMP6-210) to detect  $Ca^{2+}$  release from the ER in mushroom body Kenyon cells. Here we have expressed this probe and two others with higher  $Ca^{2+}$  affinities under GAL4 control in *Drosophila* motor neurons. We show ER-GCaMP6-210 as the most effective reporter of the three by consistently producing the largest changes in fluorescent intensity and characterize its localization and its reporting of stimulation-frequency-dependent ER  $Ca^{2+}$  fluxes in axon and presynaptic terminals. We then use it to show perturbation of  $Ca^{2+}$  handling in *Drosophila* in which ER organization is disrupted by loss of HSP-related ER-modeling proteins.

## MATERIALS AND METHODS

### Gene Constructs

The *pUASTattB* vector (Bischof et al., 2007) was previously modified to include *attR* sites and the *ccdB* gene to make it compatible with the Gateway cloning system (Invitrogen) (Moreau et al., 2014). We further modified this vector, increasing the number of GAL4-binding sites from 5 to 17, to generate *p17xUASTattB*, and increase GAL4-dependent gene expression (Supplementary Datasheet 2). To generate *p17xUASTattB-ER-GCaMP6-210*, we PCR-amplified a fragment encoding GCaMP210-KDEL fused to a calreticulin signal peptide, from Addgene plasmid *ER-GCaMP6-210* (de Juan-Sanz et al., 2017) (Table 1), while adding *attB1* and *attB2* sites to its 5' and 3' ends to enable it to integrate into *p17xUASTattB* using the Gateway cloning system (Supplementary Datasheet 2). To generate *p17xUASTattB-CEPIA3-ER* and *p17xUASTattB-CEPIA4-ER*, we PCR-amplified the CEPIA coding region from Addgene plasmids *pCMV CEPIA3mt* and *pCMV CEPIA4mt* (Suzuki et al., 2014) (Table 1), while adding *attB1* and a BiP signal sequence to the

**TABLE 1** | Stocks and plasmids used in this work.

<i>Drosophila</i> stock genotype	RRID	Source/References
<i>y w</i> ; +; <i>17xUASTattB-ER-GCaMP6-210(attP86Fb)</i>	–	This paper
<i>y w</i> ; +; <i>17xUASTattB-CEPIA3-ER(attP86Fb)</i>	–	This paper
<i>y w</i> ; +; <i>17xUASTattB-CEPIA4-ER(attP86Fb)</i>	–	This paper
<i>w<sup>1118</sup></i> ; +; <i>UAS-tdTomato:Sec61β(attP2)</i>	BDSC_64747	Summerville et al., 2016
<i>w</i> ; <i>UAS-Sturkopf:GFP</i> ; + (Formerly <i>UAS-CG9186:GFP</i> )	–	(Thiel et al., 2013) Yalçın et al., 2017
<i>w</i> ; +; <i>UAS-jRCaMP1b(VK00005)</i>	BDSC_63793	Dana et al., 2016
<i>w</i> ; <i>Rtnl1<sup>-</sup> ReepA<sup>-</sup> ReepB<sup>-</sup>/CyO</i> ; +	BDSC_77904	Yalçın et al., 2017
<i>w</i> ; <i>ReepA<sup>+</sup></i> ; + (WT control)	–	Yalçın et al., 2017
<i>w<sup>1118</sup></i> ; +; <i>Dpr-GMR94G06-GAL4(attP2)</i>	BDSC_40701	Pfeiffer et al., 2008; Perez-Moreno and O'Kane, 2019
<i>w<sup>1118</sup></i> ; +; <i>FMR-GMR27E09-GAL4(attP2)</i>	BDSC_49227	Pfeiffer et al., 2008; Perez-Moreno and O'Kane, 2019
<b>Plasmid</b>		
<i>ER-GCaMP6-210</i>	Addgene_86919	Tim Ryan (de Juan-Sanz et al., 2017)
<i>pCMV CEPIA3mt</i>	Addgene_58219	Masamitsu Iino (Suzuki et al., 2014)
<i>pCMV CEPIA4mt</i>	Addgene_58220	Masamitsu Iino (Suzuki et al., 2014)
<i>p17xUASTattB</i>	–	This paper
<i>p17xUASTattB-ER-GCaMP6-210</i>	–	This paper
<i>p17xUASTattB-CEPIA3-ER</i>	–	This paper
<i>p17xUASTattB-CEPIA4-ER</i>	–	This paper

5' end, and HDEL and *attB2* to the 3' end [BiP and HDEL ER-targeting as in Summerville et al. (2016)], and then integrating it into *p17xUASTattB* (Supplementary Datasheet 2).

### *Drosophila* Genetics

*p17xUASTattB-ER-GCaMP6-210*, *p17xUASTattB-CEPIA3-ER*, and *p17xUASTattB-CEPIA4-ER* were injected into *Drosophila* embryos and integrated at landing site *attP86Fb* (Bischof et al., 2007) using phiC31 integrase-mediated integration, by the University of Cambridge Genetics Department injection service. Other fly stocks used can be found in Table 1.

### Histology

Third instar larvae were dissected in ice-cold  $Ca^{2+}$ -free HL3 solution (Stewart et al., 1994). HL3 was then replaced with PBS and larvae fixed for 10 min in PBS with 4% formaldehyde. Fixed preparations were mounted in Vectashield (Vector Laboratories), and images were collected using EZ-C1 acquisition software (Nikon) on a Nikon Eclipse C1si confocal microscope (Nikon Instruments, United Kingdom). Images were captured using a 40×/1.3 NA oil objective.

### Live Imaging

Third instar larvae were dissected in ice-cold Schneider's insect medium (Sigma). Before imaging, Schneider's medium was

replaced with HL3 containing (in mM) 70 NaCl, 5 KCl, 0.5 MgCl<sub>2</sub>, 10 NaHCO<sub>3</sub>, 115 sucrose, 5 trehalose, 5 HEPES, 1 CaCl<sub>2</sub> and 7 L-glutamic acid, pH  $\sim 7.2 \pm 0.05$ . The ER luminal response to electrical stimulation was sensitive to Mg<sup>2+</sup>, with only very small or no responses elicited in HL3 containing 20 mM MgCl<sub>2</sub>, which was used for fixed samples; a low-Mg<sup>2+</sup> HL3 solution (0.5 mM MgCl<sub>2</sub>) gave much more reliable responses.

Segmental nerves were cut with dissection scissors and then drawn by suction into a heat-polished glass pipette,  $\sim 10 \mu\text{m}$  internal diameter (Macleod et al., 2002), which was connected to a stimulator and train generator [DS2A-MK.II Constant Voltage Stimulator and DG2A Train/Delay Generator (Digitimer, Welwyn Garden City, United Kingdom)] to deliver supra-threshold electrical pulses ( $\sim 5 \text{ V}$ ). Larval neuromuscular junction (LMJ) responses were recorded in abdominal segments A4–A6. After 10 s of baseline image acquisition, 400- $\mu\text{s}$  impulses were delivered for 2 s at a range of frequencies. The interval between different stimulation frequencies was  $\sim 60 \text{ s}$ , or until ER lumen fluorescence returned to baseline levels (whichever was longer).

Wide-field Ca<sup>2+</sup> imaging was performed on an upright Zeiss Axioskop2 microscope with Optosplit II (Cairn) using a 40 $\times$  NA 1.0 water-immersion objective (W Plan-Apochromat 40 $\times$ /1.0 DIC M27), a 2 $\times$  C-Mount Fixed Focal Length Lens Extender (Cairn, Faversham, United Kingdom) and an Andor EMCCD camera (Model iXon Ultra 897\_BV, 512  $\times$  512 pixels, Andor Technology, Belfast, United Kingdom) at 10 frames per second, 100 ms exposure, and EM gain level 100. Imaging data were acquired using Micro-Manager (Edelstein et al., 2014) and saved as multi-layer tif files before analysis using ImageJ Fiji<sup>1</sup> (Schindelin et al., 2012).

## Image Analysis and Figure Preparation

Confocal microscopy images of fixed samples were collected using EZ-C1 acquisition software on a Nikon Eclipse C1si confocal microscope. Images were analyzed and processed using ImageJ Fiji<sup>2</sup> (Schindelin et al., 2012). Wide-field live images were opened in ImageJ Fiji, and channels were individually bleach-corrected (simple ratio, background intensity = 0). Fluorescent intensity time courses were obtained for an ROI (region of interest) traced around the entire NMJ, or axon segment, in each frame in a given data set using Time Series Analyzer V3 plugin, averaging the fluorescence in the ROI. The time courses were saved as txt files and fed into R scripts written by the authors to obtain the resting fluorescence data (averaged 30 frames before stimulus) and the  $\Delta F/F$  data (Supplementary Datasheet 3). Graphs were generated using GraphPad Prism 8. Figures were made using Adobe Illustrator.

## Statistical Analysis

Data were analyzed in GraphPad Prism, using 2-way ANOVA, unpaired two-tailed Student's *t*-tests; graphs show mean  $\pm$  SEM or Mann–Whitney U tests (for data not normally distributed); graphs show median with interquartile range. Pearson's

correlation was used to examine relationships between datasets. Sample sizes are reported in figures.

## RESULTS

### The ER Luminal Ca<sup>2+</sup> Evoked Response Is More Delayed and Sustained Compared to the Cytoplasmic Response

To monitor Ca<sup>2+</sup> flux in the ER lumen, we generated transgenic flies that encoded ER-GCaMP6-210 (de Juan-Sanz et al., 2017), a GCaMP6 sensor fused to a signal peptide and ER retention signal, with a Ca<sup>2+</sup> affinity optimized for the relatively high [Ca<sup>2+</sup>] in ER lumen. ER-GCaMP6-210 localization in presynaptic terminals largely overlapped with the ER marker tdTomato:Sec61 $\beta$  (Figure 1A), being more restricted than cytoplasmic jRCaMP1b (Figure 1B; see comparison to ER marker Sturkopf:GFP, previously known as CG9186:GFP), consistent with localization to the ER lumen. To test the response of the sensor to neuronal activation we electrically stimulated the nerve. The cytoplasmic Ca<sup>2+</sup> response quickly reached a peak in the first couple of seconds following stimulation, and decayed back to resting levels over several seconds. In contrast, the ER-GCaMP6-210 luminal response increased more slowly, reaching a peak five or more seconds following stimulation, with a slow return to resting levels, in some cases over minutes (Figures 2A,B and Supplementary Video 1), in keeping with the slower dynamics reported previously for these constructs (de Juan-Sanz et al., 2017). Cytoplasmically, jRCaMP1b and GCaMP6f have similar kinetics in neurons as reported previously, with just a slightly slower half decay time (0.6 s) for jRCaMP1b (Dana et al., 2016), compared to GCaMP6f (0.4 s) (Chen et al., 2013) at 10 Hz. In around 10% of nerves, usually at higher stimulation frequencies, we alternatively (or sometimes additionally) observed small, sharp decreases in ER luminal fluorescence immediately following stimulation. This decrease was followed by a quick return to baseline fluorescence or by a slow increase in fluorescence as described above. This short-term decrease in fluorescence was observed more frequently in the axon than at the NMJ. There did not appear to be anything notably different in the cytoplasmic flux in these instances, compared to when the ER flux showed only an increase in fluorescence (Figure 2A and Supplementary Datasheet 1). Together, these data suggest a slower and somewhat less predictable ER Ca<sup>2+</sup> flux, compared to the cytoplasmic flux in axons and NMJs of motor neurons.

### ER Luminal Sensor With Affinity Closest to Predicted ER Luminal [Ca<sup>2+</sup>] Shows the Strongest Response

Since the high surface/volume ratio of the small ER tubules of axons might potentially make them more susceptible than other ER regions to leakage of Ca<sup>2+</sup> to the cytosol, we generated transgenic flies carrying two additional ER luminal sensors with higher Ca<sup>2+</sup> affinities. The highest affinity sensor, CEPIA3-ER ( $K_d = 11 \mu\text{M}$ ), showed very

<sup>1</sup><https://fiji.sc>

<sup>2</sup>See footnote 1.

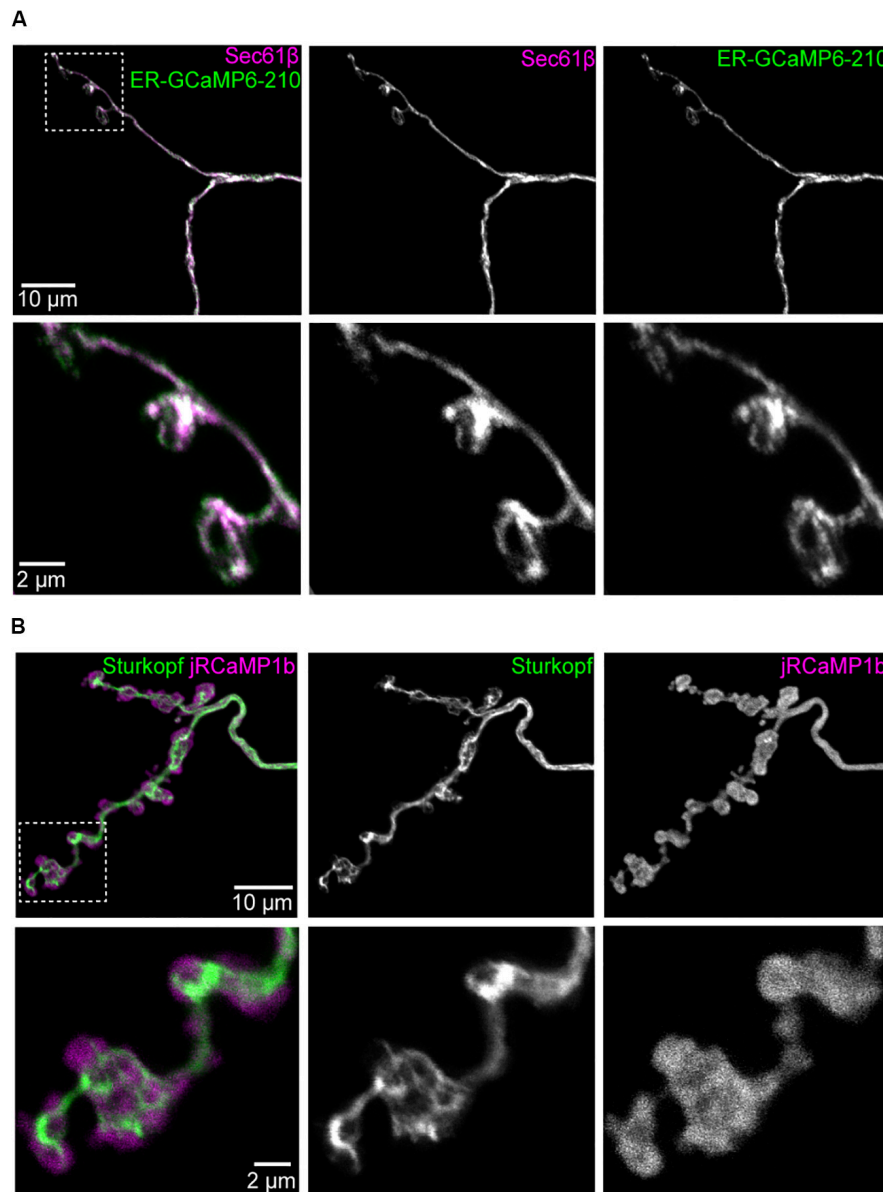
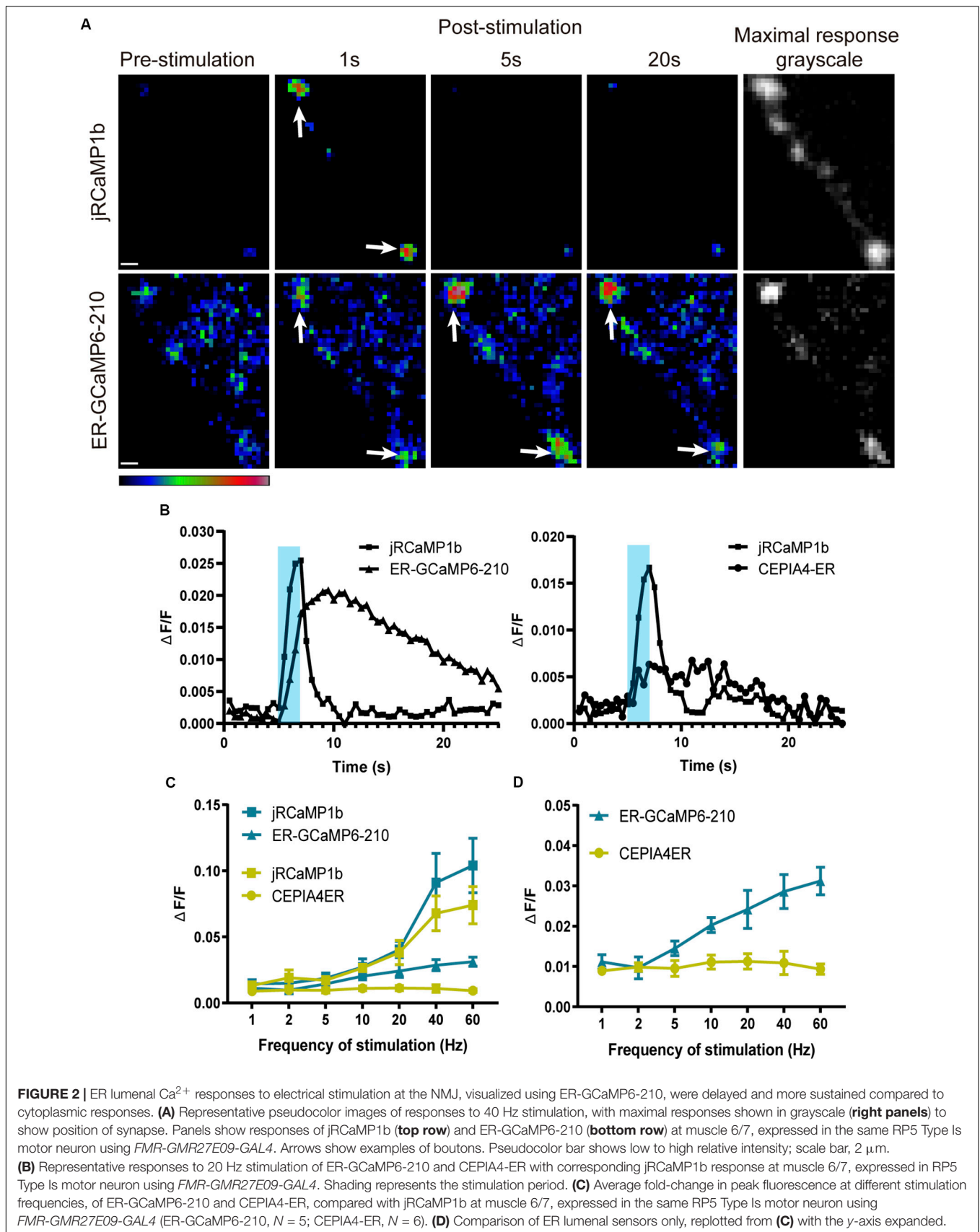


**FIGURE 1 |** The ER luminal sensor ER-GCaMP6-210 has an overlapping distribution with ER at the neuromuscular junction. Panels show markers in Ib boutons at muscle 1 NMJ, segment A2, expressed using *Dpr-GMR94G06-GAL4*; all images are maximum intensity projections of confocal stacks. **(A)** Overlap of ER-GCaMP6-210 and ER membrane marker tdTomato:Sec61β. **(B)** jRCaMP1b is more broadly distributed than ER membrane marker Sturkopf:GFP. Magnified views of each inset are in respective lower rows.

small or no responses at multiple NMJs of seven larval preparations, even when a robust cytoplasmic response was elicited (not shown); CEPIA4-ER ( $K_d = 59 \mu\text{M}$ ) usually showed a small response at most frequencies. ER-GCaMP6-210 ( $K_d = 210 \mu\text{M}$ ) produced the most consistent response, and the magnitude of its response increased with increasing stimulation frequency (**Figures 2B–D**). As sensors with a  $K_d$  that approximates the surrounding  $[\text{Ca}^{2+}]$  are best suited as reporters, this is consistent with the estimated resting neuronal ER luminal  $[\text{Ca}^{2+}]$  of 150–200  $\mu\text{M}$  reported previously (de Juan-Sanz et al., 2017).

### The Axonal Cytoplasmic Evoked Response Is Smaller Compared to NMJ Response, Whereas the ER Luminal Evoked Response Is Consistent Across Locations

As we were interested to see if we could observe  $\text{Ca}^{2+}$  signals along the length of the axon, we used *FMR-GMR27E09-GAL4* to record in the two Type IIs motor neurons per hemisegment where it drives expression: RP2 and RP5, which together innervate several NMJs (Perez-Moreno and O’Kane, 2019). We compared



several axonal and NMJ locations within a muscle hemisegment (**Supplementary Datasheet 1**). Motor neuron RP2 (also known as ISN-Is) innervates dorsal muscles, and we recorded from its NMJ boutons at muscle 1, and from two axonal locations: the “entry” point at which the axon starts to cross the muscles as it emerges from the ventral nerve cord, and more laterally as it passes over muscle 4. Motor neuron RP5 (also known as ISN b/d) innervates ventral muscles, and we recorded from its NMJ at muscle 6/7, and from one axonal location, the “entry” point, as defined for motor neuron RP2 (**Supplementary Datasheet 1** and **Supplementary Video 2**). *Dpr-GMR94G06-GAL4* drives expression in the aCC Type Ib motor neuron (also known as MN1-Ib), which innervates muscle 1 (Perez-Moreno and O’Kane, 2019). The responses of both cytosolic and luminal sensors at the aCC muscle 1 NMJ boutons were comparable to those in RP2 at the same muscle (**Figures 3A,B**), suggesting a comparable action potential response between the two neuronal types. Fluorescence of the sensors driven by *Dpr-GMR94G06-GAL4* in the axons of the Type Ib aCC neuron was too dim to obtain reliable evoked responses, which may be due to a relatively small diameter of its axon, and hence relatively low amounts of sensors at this subcellular location.

The evoked cytoplasmic NMJ and axonal  $\text{Ca}^{2+}$  responses were both comparable between the two Type Is motor neurons, although axonal responses were consistently smaller than NMJ responses whereas ER luminal evoked responses were consistent across all NMJ and axonal locations (**Figure 3C**). This did not appear to be due to alterations in ER volume as resting fluorescence was consistent across locations (**Supplementary Datasheet 1**). Both cytoplasmic and ER luminal responses reached peak fluorescence on similar timescales across locations (**Figure 3D**), suggesting that the observed responses were due to  $\text{Ca}^{2+}$  flux across the plasma membrane, and not a propagation of  $\text{Ca}^{2+}$  down the axon. The ER luminal response appeared in general not to be influenced by the cytoplasmic response; most locations showed no correlation of peak  $\Delta F/F$  between ER lumen and cytosol, apart from RP2 axon at entry point (**Figures 3E,F** and **Table 2**). This suggests a more complex transfer of  $\text{Ca}^{2+}$  within and between intracellular compartments, than simply a flow of  $\text{Ca}^{2+}$  from cytosol to ER lumen.

### ***Rtnl1*<sup>-</sup> *ReepA*<sup>-</sup> *ReepB*<sup>-</sup> Mutants Display an Increased ER Luminal Evoked Response Compared to Wild Type (WT)**

*Rtnl1*<sup>-</sup> *ReepA*<sup>-</sup> *ReepB*<sup>-</sup> mutant larvae have a disrupted axonal ER network, with larger and fewer tubules, and occasional fragmentation (Yalçın et al., 2017). To test whether these ER changes had functional consequences, we used *Dpr-GMR94G06-GAL4* to examine the cytoplasmic and ER lumen evoked responses at muscle 1 NMJ in these mutants. Mutant NMJs showed an increased evoked response compared to WT in the ER lumen, but not in the cytoplasm (**Figures 4A,B**). There was no significant difference in lumen resting fluorescence between mutant and WT (**Figure 4C**).

There was no correlation between cytoplasmic and ER luminal evoked responses in either mutant or WT at 40 Hz

(**Supplementary Datasheet 1**), supporting the finding in **Figure 3** of a more complex intracellular transfer of calcium. It has been reported that ER lumen  $[\text{Ca}^{2+}]$  affects presynaptic cytoplasmic  $\text{Ca}^{2+}$  flux (de Juan-Sanz et al., 2017); however, we found no correlation here between resting ER fluorescence and peak cytoplasmic fluorescence, in either WT or mutant stimulated at 40 Hz (**Supplementary Datasheet 1**). The time-to-peak in the cytoplasm or ER lumen was not significantly different between mutant and WT at 40 Hz (**Supplementary Datasheet 1**). The time for decay to half-maximal in the cytoplasm was also not significantly different between mutant and WT at 40 Hz (**Supplementary Datasheet 1**). This parameter was not measured in the ER lumen due to the slow temporal dynamics of this flux.

These data suggest a significant increase in ER luminal evoked responses in *Rtnl1*<sup>-</sup> *ReepA*<sup>-</sup> *ReepB*<sup>-</sup> mutants compared to WT, with no change in ER luminal resting fluorescence levels, no corresponding change in the cytoplasmic evoked response, and no change in the temporal dynamics of the response.

## **DISCUSSION**

Direct measurement of ER luminal  $\text{Ca}^{2+}$  dynamics is essential for reporting on the physiological and pathophysiological responses of the ER network. An ER luminal *UAS-GECl*, ER-GCaMP6-210, provided the most robust responses in *Drosophila* motor neurons (**Figure 2**), in keeping with results in mammalian hippocampal neurons (de Juan-Sanz et al., 2017). Handler et al. (2019) also expressed this sensor in transgenic flies using a 10× UAS vector, and used these to detect  $\text{Ca}^{2+}$  release from the ER in mushroom body Kenyon cells. Our work provides a more detailed characterization of the responses of this sensor to a range of stimulation frequencies, as well as providing an additional 17xUAS vector that we predict allows higher expression of the sensor.

In mutant *Drosophila* lacking various ER-shaping HSP protein homologs, we previously found decreased ER levels compared to WT, or occasional discontinuity of the ER network (Yalçın et al., 2017). As sustained discontinuity could potentially disrupt long-range ER communication along the axon, we wanted to investigate if we could record  $\text{Ca}^{2+}$  fluxes in WT axons. We analyzed both cytoplasmic and ER luminal  $\text{Ca}^{2+}$  fluxes, at three axonal recording positions across two neurons. The amplitude of the ER luminal evoked response was similar in axons and at the NMJ; however, cytoplasmic evoked responses were smaller in axons compared to the NMJ. Even though  $\text{Ca}^{2+}$  would be fluxing across the ER membrane in response to stimulation, it appears that the two signals do not influence each other in most cases (**Figure 3**).

While we observe  $\text{Ca}^{2+}$  signals along the length of motor axons, we do not find any indication of propagation via a  $\text{Ca}^{2+}$  wave. Propagation speeds for  $\text{Ca}^{2+}$  waves in dendrites have been measured at 60–90  $\mu\text{m/s}$  (Nakamura et al., 2002), with a rapid luminal  $\text{Ca}^{2+}$  diffusion through dendritic ER at  $\sim 30 \mu\text{m/s}$  (Choi et al., 2006). Here we find no evidence for any spatial differences in the time to peak fluorescence

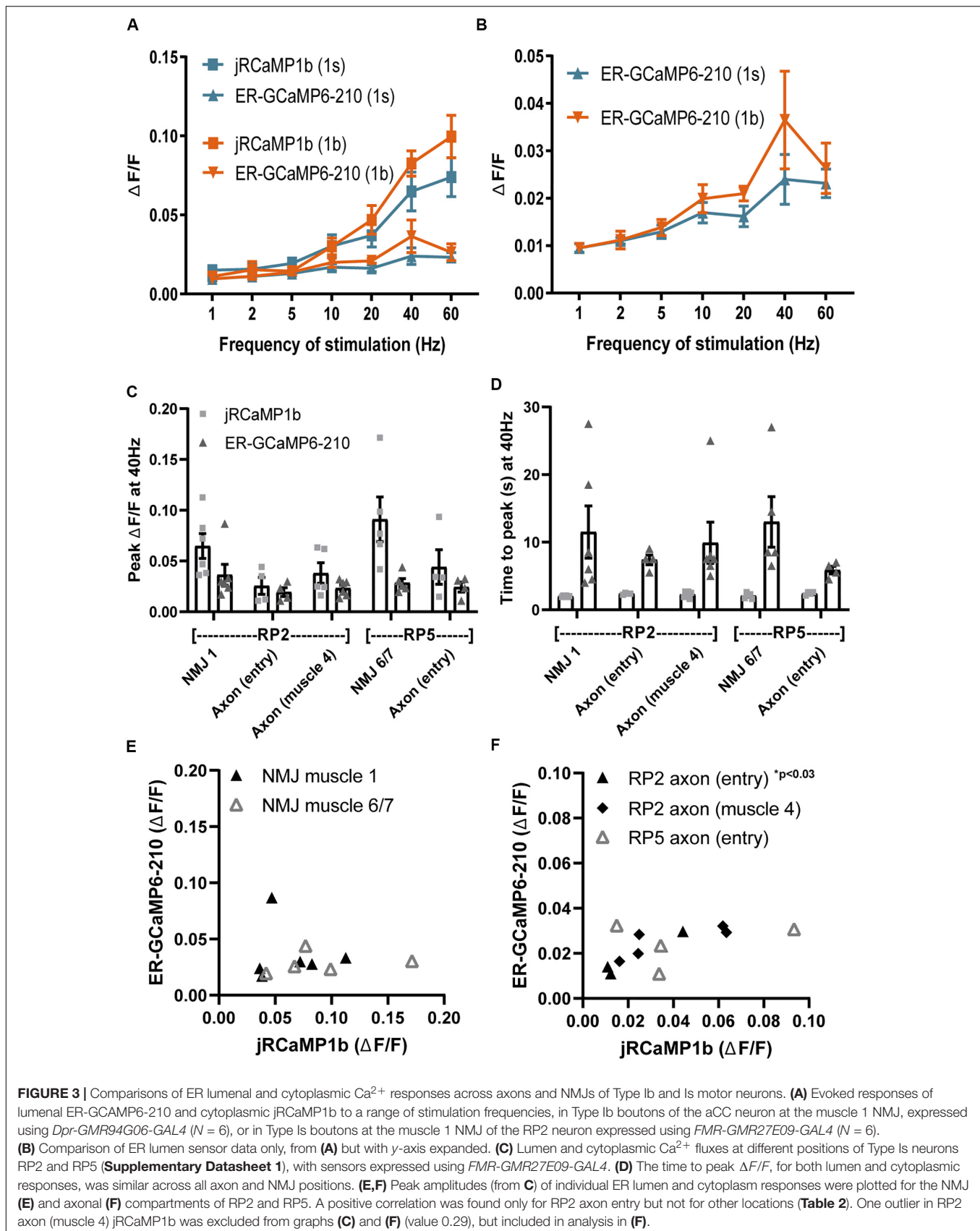


**TABLE 2** | Correlation analysis of peak  $\Delta F/F$  between ER lumen and cytosol in NMJ and axons using Pearson's correlation coefficient.

<i>FMR-GMR27E09</i> neuronal location	<i>r</i>	<i>p</i>	<i>N</i> (larvae)
RP2 NMJ muscle 1	0.10	0.85	6
RP5 NMJ muscle 6/7	0.21	0.73	5
RP2 axon (entry)	0.98	0.02*	4
RP2 axon (muscle 4)	0.50	0.32	6
RP5 axon (entry)	0.23	0.77	4

\**P* < 0.05.

between different axon positions and the NMJ, both for ER lumen and cytoplasmic evoked responses (Figure 3); in a typical video frame width of 100  $\mu\text{m}$  (e.g., Supplementary Datasheet 1) we should easily detect propagation at these speeds with our frame rate of 10 Hz. The instantaneous spread of  $\text{Ca}^{2+}$  responses that we observe is more consistent with them being a consequence of the action potentials generated by stimulation, which propagate so fast that we cannot resolve their spread using our optical recording. Detection of  $\text{Ca}^{2+}$  waves that propagate along the ER membrane or through the lumen would probably require recording of ER  $\text{Ca}^{2+}$  fluxes in the absence of action potentials.

Although the cytoplasmic evoked responses of *Rtn1<sup>-</sup> ReepA<sup>-</sup> ReepB<sup>-</sup>* mutants were normal, the ER luminal evoked responses were significantly larger than WT (Figure 4). This did not appear to be due to increased resting ER luminal  $[\text{Ca}^{2+}]$  since resting fluorescence levels showed no significant difference between genotypes, for either ER or cytoplasmic sensors.

In the simplest interpretation, the presynaptic ER lumen appears to take up more  $\text{Ca}^{2+}$  on stimulation in the *Rtn1<sup>-</sup> ReepA<sup>-</sup> ReepB<sup>-</sup>* mutant compared to WT. Since cytoplasmic  $\text{Ca}^{2+}$  responses are unaffected in mutants, increased cytosolic  $\text{Ca}^{2+}$  cannot be an explanation for the increased ER response in mutants, implying that the increased ER response is due to intrinsic changes in  $\text{Ca}^{2+}$ -handling properties of the mutant ER, consistent with the roles of reticulon and REEP proteins in directly shaping ER architecture. The change in shape and composition of the ER tubules may change their flexibility (Georgiades et al., 2017) and effectiveness of ER tubule contraction (Holcman et al., 2018), hence a decrease in active flow, thereby slowing the redistribution, and presenting as a transient increase in ER luminal  $\text{Ca}^{2+}$ . However, as ER tubules have a larger diameter in mutant ER (Yalçın et al., 2017), this would work against this theory, as the larger tubules should enable active flow (Holcman et al., 2018). Alternatively, expression of ER  $\text{Ca}^{2+}$  proteins may be affected, such as the ER  $\text{Ca}^{2+}$  release channel RyR, highly expressed at axonal boutons (Sharp et al., 1993). If its expression levels were decreased, or its distribution altered, this could account for the lack of  $\text{Ca}^{2+}$  able to escape the lumen and explain the transient increase in  $\text{Ca}^{2+}$  uptake observed on stimulation. Increased uptake of  $\text{Ca}^{2+}$  by mutant ER does not lead to decreased cytoplasmic  $[\text{Ca}^{2+}]$ ; however, we might not detect very local reductions in  $[\text{Ca}^{2+}]$  close to the ER, if masked by excess cytoplasmic fluorescence away from its immediate vicinity. Increasing bath  $[\text{Ca}^{2+}]$  can

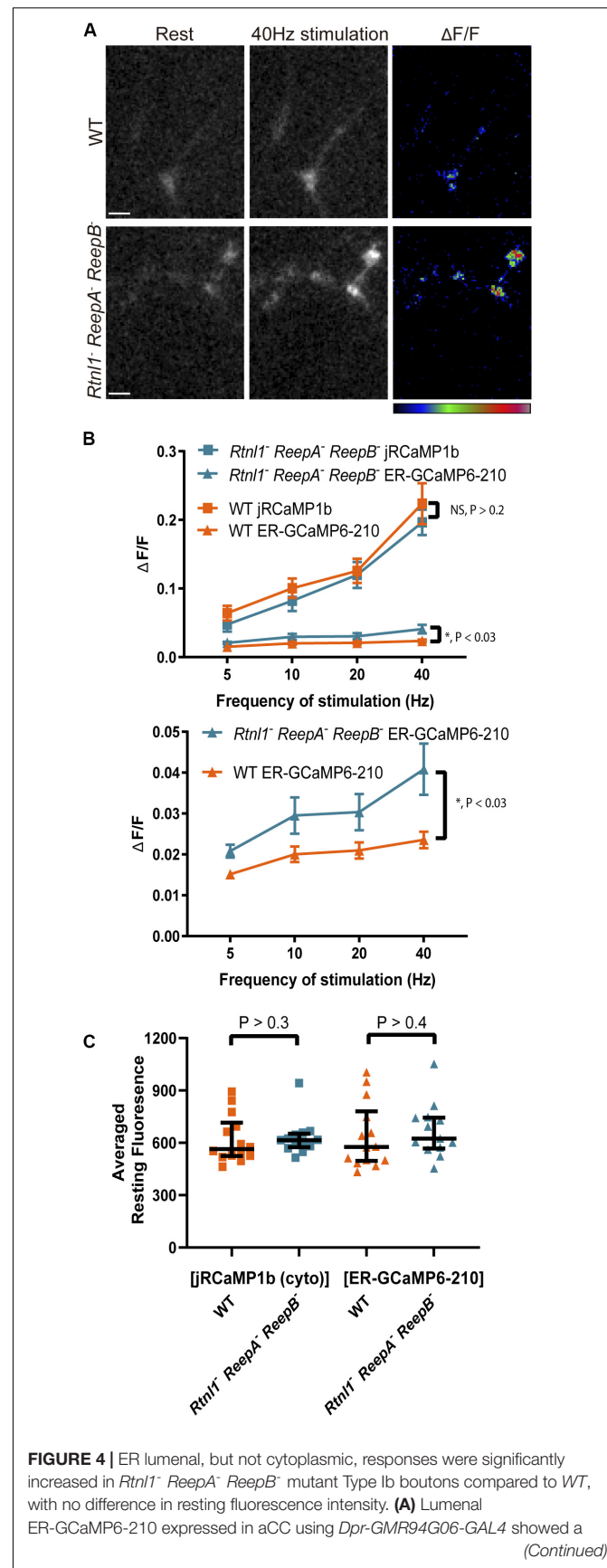


**FIGURE 4 | Continued**

larger evoked response in Type Ib NMJs at muscle 1 in mutants, compared to WT; 40 Hz stimulation panel shows the maximum response of the given GECI following stimulation. GECIs were co-expressed in the same neuron.

Pseudocolor bar (for  $\Delta F/F$  panels) shows low to high  $\Delta F/F$ ; scale bar, 5  $\mu\text{m}$ .

**(B)** There was no significant difference between mutant ( $N = 13$  larvae) and WT ( $N = 14$  larvae) in cytoplasmic responses (jRCaMP1b) at these boutons stimulated over a range of frequencies, but there was a significant increase in the ER lumenal response (2-way ANOVA). The lower graph shows the ER lumenal response only, with the y-axis expanded. **(C)** There was no significant effect of the triple mutant on the resting fluorescence intensity (from the 40 Hz recording) of either sensor (Mann–Whitney U test).

rescue transmitter release phenotypes in *atl* and *Rtnl1* mutants (Summerville et al., 2016); reducing bath  $[\text{Ca}^{2+}]$  in our setup might reveal cytoplasmic dysfunction not apparent at higher bath  $[\text{Ca}^{2+}]$ .

Could the increased ER lumenal  $\text{Ca}^{2+}$  responses in mutants have any effects on cell physiology, if there is no corresponding increase in  $[\text{Ca}^{2+}]$  in the cytoplasm, where many  $\text{Ca}^{2+}$  effectors reside? There are  $\text{Ca}^{2+}$  effectors in the ER lumen such as calreticulin (Opas et al., 1991), although the protein-folding chaperone role of calreticulin is more likely to place its main function in rough rather than smooth ER. However, altered lumenal  $\text{Ca}^{2+}$  responses could also affect physiology of organelles that obtain  $\text{Ca}^{2+}$  from the ER, including mitochondria and endo/lysosomal organelles (Raffaello et al., 2016). These effects could endure well beyond the original train of action potentials, due to the slow kinetics of  $\text{Ca}^{2+}$  uptake and release by the ER, with lumenal  $[\text{Ca}^{2+}]$  not always returning to baseline during our recordings. Furthermore, aberrant ER  $\text{Ca}^{2+}$  handling has been postulated as a trigger for neurodegeneration, so what we are observing may well reflect deleterious changes in cellular health (Stutzmann and Mattson, 2011; Ureshino et al., 2019). In support of our findings, mutation or knockdown of genes with a role in ER shaping, including *atl*, *Rtnl1*, and *VAP*, also affect aspects of presynaptic function including neurotransmitter release and synaptic vesicle density, and the cytoplasmic presynaptic  $\text{Ca}^{2+}$  response (Summerville et al., 2016; De Gregorio et al., 2017; Lindhout et al., 2019). Given the number of HSP genes whose products localize to ER (Montenegro et al., 2012; Blackstone, 2018) and could therefore affect  $\text{Ca}^{2+}$  dynamics, altered  $\text{Ca}^{2+}$  handling in axons or axonal terminals could potentially be a contributory factor to HSP pathology. Taken together, these data strongly suggest a role for ER in modulating presynaptic function and highlight the importance of having an intact, functional ER network.

## CONCLUSION

In conclusion, we have demonstrated the use of ER lumenally targeted GECIs for use in *Drosophila*, successfully recording fluxes at both the NMJ and the axon. We have demonstrated the utility of these sensors in identifying functional differences between WT and *Rtnl1*<sup>-</sup> *ReepA*<sup>-</sup> *ReepB*<sup>-</sup> mutant flies, whose axonal ER network it

is known to be affected. We anticipate these will be useful additions to a *Drosophila*  $\text{Ca}^{2+}$  imaging toolkit in the future, to further our understanding of HSP and neurodegeneration more broadly.

## DATA AVAILABILITY STATEMENT

This article contains previously unpublished data. Underpinning data are available on: <https://www.repository.cam.ac.uk/>, DOI link: doi: 10.17863/CAM.55394.

## AUTHOR CONTRIBUTIONS

MO performed all the cloning and  $\text{Ca}^{2+}$  imaging experiments. MO and CO'K designed the experiments. JP-M performed the confocal imaging acquisition. JO'S performed the preliminary experiments and contributed to the data analysis. TW provided the initial training and support for  $\text{Ca}^{2+}$  imaging experiments and assisted in the experimental design. The manuscript was written by MO and CO'K with comments and edits by JP-M, TW, and JO'S. All authors contributed to the article and approved the submitted version.

## FUNDING

This work was supported by grants BB/L021706 from the UK Biotechnology and Biological Sciences Research Council and MR/S011226 from the UK Medical Research Council to CO'K. MO was supported by a Newton International Fellowship (NF150362) from The Royal Society and a Marie Skłodowska-Curie Fellowship (701397) from the European Commission. JP-M was supported by a Marie Skłodowska-Curie Fellowship (745007) from the European Commission. TW was supported by a David Phillips Fellowship from the Biotechnology and Biological Sciences Research Council (BBSRC) (BB/L024667/1) and later by the College of Biological Sciences, University of Minnesota.

## ACKNOWLEDGMENTS

We thank the Department of Genetics Fly Facility, University of Cambridge, for providing the *Drosophila* microinjection service, Timothy Ryan for providing the FCK(1.3)GW-ER-GCaMP6-210 plasmid, and Bloomington *Drosophila* Stock Centre for the stocks. This manuscript has been released as a pre-print at bioRxiv (Oliva et al., 2020).

## SUPPLEMENTARY MATERIAL

The Supplementary Material for this article can be found online at: <https://www.frontiersin.org/articles/10.3389/fnins.2020.00816/full#supplementary-material>

## REFERENCES

- Bischof, J., Maeda, R. K., Hediger, M., Karch, F., and Basler, K. (2007). An optimized transgenesis system for *Drosophila* using germ-line-specific phiC31 integrases. *Proc. Natl. Acad. Sci. U.S.A.* 104, 3312–3317. doi: 10.1073/pnas.0611511104
- Blackstone, C. (2018). Converging cellular themes for the hereditary spastic paraplegias. *Curr. Opin. Neurobiol.* 51, 139–146. doi: 10.1016/j.conb.2018.04.025
- Chen, T. W., Wardill, T. J., Sun, Y., Pulver, S. R., Renninger, S. L., Baohan, A., et al. (2013). Ultrasensitive fluorescent proteins for imaging neuronal activity. *Nature* 499, 295–300. doi: 10.1038/nature12354
- Choi, Y. M., Kim, S. H., Chung, S., Uhm, D. Y., and Park, M. K. (2006). Regional interaction of endoplasmic reticulum Ca<sup>2+</sup> signals between soma and dendrites through rapid luminal Ca<sup>2+</sup> diffusion. *J. Neurosci.* 26, 12127–12136. doi: 10.1523/JNEUROSCI.3158-06.2006
- Dana, H., Mohar, B., Sun, Y., Narayan, S., Gordus, A., Hasseman, J. P., et al. (2016). Sensitive red protein calcium indicators for imaging neural activity. *eLife* 5:e12727 doi: 10.7554/eLife.12727
- De Gregorio, C., Delgado, R., Ibacache, A., Sierralta, J., and Couve, A. (2017). *Drosophila* Atlastin in motor neurons is required for locomotion and presynaptic function. *J. Cell Sci.* 130, 3507–3516. doi: 10.1242/jcs.201657
- de Juan-Sanz, J., Holt, G. T., Schreiter, E. R., de Juan, F., Kim, D. S., and Ryan, T. A. (2017). Axonal endoplasmic reticulum Ca(2+) content controls release probability in CNS nerve terminals. *Neuron* 93, 867–881. doi: 10.1016/j.neuron.2017.01.010
- Edelstein, A. D., Tsuchida, M. A., Amodaj, N., Pinkard, H., Vale, R. D., and Stuurman, N. (2014). Advanced methods of microscope control using muManager software. *J. Biol. Methods* 1, e10–e20. doi: 10.14440/jbm.2014.36
- Fowler, P. C., and O'Sullivan, N. C. (2016). ER-shaping proteins are required for ER and mitochondrial network organization in motor neurons. *Hum. Mol. Genet.* 25, 2827–2837. doi: 10.1093/hmg/ddw139
- Georgiades, P., Allan, V. J., Wright, G. D., Woodman, P. G., Udommai, P., Chung, M. A., et al. (2017). The flexibility and dynamics of the tubules in the endoplasmic reticulum. *Sci. Rep.* 7, 16474–16484. doi: 10.1038/s41598-017-16570-4
- Handler, A., Graham, T. G. W., Cohn, R., Morantte, I., Siliciano, A. F., Zeng, J., et al. (2019). Distinct dopamine receptor pathways underlie the temporal sensitivity of associative learning. *Cell* 178, 60–75.e19. doi: 10.1016/j.cell.2019.05.040
- Holcman, D., Parutto, P., Chambers, J. E., Fantham, M., Young, L. J., Marciniak, S. J., et al. (2018). Single particle trajectories reveal active endoplasmic reticulum luminal flow. *Nat. Cell Biol.* 20, 1118–1125. doi: 10.1038/s41556-018-0192-2
- Li, J., Yan, B., Si, H., Peng, X., Zhang, S. L., and Hu, J. (2017). Atlastin regulates store-operated calcium entry for nerve growth factor-induced neurite outgrowth. *Sci. Rep.* 7–16, 43490. doi: 10.1038/srep43490
- Lindhout, F. W., Cao, Y., Kevenaar, J. T., Bodzeta, A., Stucchi, R., Boumpoutsari, M. M., et al. (2019). VAP-SCRN1 interaction regulates dynamic endoplasmic reticulum remodeling and presynaptic function. *EMBO J.* 38, e101345. doi: 10.15252/embj.2018101345
- Macleod, G. T., Hegstrom-Wojtowicz, M., Charlton, M. P., and Atwood, H. L. (2002). Fast calcium signals in *Drosophila* motor neuron terminals. *J. Neurophysiol.* 88, 2659–2663. doi: 10.1152/jn.00515.2002
- Montenegro, G., Rebelo, A. P., Connell, J., Allison, R., Babalini, C., D'Aloia, M., et al. (2012). Mutations in the ER-shaping protein reticulon 2 cause the axon-degenerative disorder hereditary spastic paraplegia type 12. *J. Clin. Invest.* 122, 538–544. doi: 10.1172/JCI60560
- Moreau, K., Fleming, A., Imarisio, S., Lopez Ramirez, A., Mercer, J. L., Jimenez-Sanchez, M., et al. (2014). PICALM modulates autophagy activity and tau accumulation. *Nat. Commun.* 5-24:4998. doi: 10.1038/ncomms5998
- Nakamura, T., Lasser-Ross, N., Nakamura, K., and Ross, W. N. (2002). Spatial segregation and interaction of calcium signalling mechanisms in rat hippocampal CA1 pyramidal neurons. *J. Physiol.* 543, 465–480. doi: 10.1113/jphysiol.2002.020362
- Oliva, M. K., Pérez-Moreno, J. J., O'Shaughnessy, J., Wardill, T. J., and O'Kane, C. J. (2020). Endoplasmic reticulum (ER) luminal indicators in *Drosophila* reveal effects of HSP-related mutations on ER calcium dynamics. *bioRxiv* [Preprint]. doi: 10.1101/2020.02.20.957696
- Opas, M., Dziak, E., Fliegel, L., and Michalak, M. (1991). Regulation of expression and intracellular distribution of calreticulin, a major calcium binding protein of nonmuscle cells. *J. Cell Physiol.* 149, 160–171. doi: 10.1002/jcp.1041490120
- O'Sullivan, N. C., Jahn, T. R., Reid, E., and O'Kane, C. J. (2012). Reticulon-like-1, the *Drosophila* orthologue of the hereditary spastic paraplegia gene reticulon 2, is required for organization of endoplasmic reticulum and of distal motor axons. *Hum. Mol. Genet.* 21, 3356–3365. doi: 10.1093/hmg/dd167
- Perez-Moreno, J. J., and O'Kane, C. J. (2019). GAL4 drivers specific for type Ib and type Is motor neurons in *Drosophila*. *G3* 9, 453–462. doi: 10.1534/g3.118.200809
- Pfeiffer, B. D., Jenett, A., Hammonds, A. S., Ngo, T. T., Misra, S., Murphy, C., et al. (2008). Tools for neuroanatomy and neurogenetics in *Drosophila*. *Proc. Natl. Acad. Sci. U.S.A.* 105, 9715–9720. doi: 10.1073/pnas.0803697105
- Raffaello, A., Mammucari, C., Gherardi, G., and Rizzuto, R. (2016). Calcium at the center of cell signaling: interplay between endoplasmic reticulum, mitochondria, and lysosomes. *Trends Biochem. Sci.* 41, 1035–1049. doi: 10.1016/j.tibs.2016.09.001
- Schindelin, J., Arganda-Carreras, I., Frise, E., Kaynig, V., Longair, M., Pietzsch, T., et al. (2012). Fiji: an open-source platform for biological-image analysis. *Nat. Methods* 9, 676–682. doi: 10.1038/nmeth.2019
- Sharp, A. H., McPherson, P. S., Dawson, T. M., Aoki, C., Campbell, K. P., and Snyder, S. H. (1993). Differential immunohistochemical localization of inositol 1,4,5-trisphosphate- and ryanodine-sensitive Ca<sup>2+</sup> release channels in rat brain. *J. Neurosci.* 13, 3051–3063. doi: 10.1523/jneurosci.13-07-03051.1993
- Stewart, B. A., Atwood, H. L., Renger, J. J., Wang, J., and Wu, C. F. (1994). Improved stability of *Drosophila* larval neuromuscular preparations in haemolymph-like physiological solutions. *J. Comp. Physiol. A* 175, 179–191. doi: 10.1007/bf00215114
- Stutzmann, G. E., and Mattson, M. P. (2011). Endoplasmic reticulum Ca(2+) handling in excitable cells in health and disease. *Pharmacol. Rev.* 63, 700–727. doi: 10.1124/pr.110.003814
- Summerville, J. B., Faust, J. F., Fan, E., Pendin, D., Daga, A., Formella, J., et al. (2016). The effects of ER morphology on synaptic structure and function in *Drosophila melanogaster*. *J. Cell Sci.* 129, 1635–1648. doi: 10.1242/jcs.184929
- Suzuki, J., Kanemaru, K., Ishii, K., Ohkura, M., Okubo, Y., and Iino, M. (2014). Imaging intraorganellar Ca<sup>2+</sup> at subcellular resolution using CEPIA. *Nat. Commun.* 5:4153. doi: 10.1038/ncomms5153
- Thiel, K., Heier, C., Haberl, V., Thul, P. J., Oberer, M., Lass, A., et al. (2013). The evolutionarily conserved protein CG9186 is associated with lipid droplets, required for their positioning and for fat storage. *J. Cell Sci.* 126, 2198–2212. doi: 10.1242/jcs.120493
- Ureshino, R. P., Erustes, A. G., Bassani, T. B., Wachilewski, P., Guarache, G. C., Nascimento, A. C., et al. (2019). The interplay between Ca(2+) signaling pathways and neurodegeneration. *Int. J. Mol. Sci.* 20:6004. doi: 10.3390/ijms20236004
- Yalçın, B., Zhao, L., Stofanko, M., O'Sullivan, N. C., Kang, Z. H., Roost, A., et al. (2017). Modeling of axonal endoplasmic reticulum network by spastic paraplegia proteins. *eLife* 6:e23882. doi: 10.7554/eLife.23882

**Conflict of Interest:** The authors declare that the research was conducted in the absence of any commercial or financial relationships that could be construed as a potential conflict of interest.

The reviewer BH declares that the endorsement is based on his professional opinion and it is not an endorsement by the US government.

Copyright © 2020 Oliva, Pérez-Moreno, O'Shaughnessy, Wardill and O'Kane. This is an open-access article distributed under the terms of the Creative Commons Attribution License (CC BY). The use, distribution or reproduction in other forums is permitted, provided the original author(s) and the copyright owner(s) are credited and that the original publication in this journal is cited, in accordance with accepted academic practice. No use, distribution or reproduction is permitted which does not comply with these terms.